Journal Pre-proofs

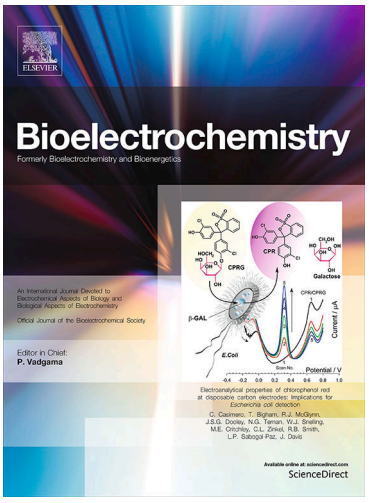

Nanostructured functional peptide films and their application in C-reactive protein immunosensors

Julia P. Piccoli, Andrey C. Soares, Osvaldo N. Oliveira Jr, Eduardo M. Cilli

PII: S1567-5394(20)30615-0
DOI: https://doi.org/10.1016/j.bioelechem.2020.107692
Reference: BIOJEC 107692

To appear in: *Bioelectrochemistry*

Received Date: 23 April 2020
Revised Date: 25 October 2020
Accepted Date: 27 October 2020

Please cite this article as: J.P. Piccoli, A.C. Soares, O.N. Oliveira Jr, E.M. Cilli, Nanostructured functional peptide films and their application in C-reactive protein immunosensors, *Bioelectrochemistry* (2020), doi: https://doi.org/10.1016/j.bioelechem.2020.107692

Nanostructured functional peptide films and their application in C-reactive protein immunosensors

Julia P. Piccoli[a†*], Andrey C. Soares[a,b], Osvaldo N. Oliveira Jr[a,*], Eduardo M. Cilli[c,*]

[a]São Carlos Institute of Physics, University of São Paulo, 13566-590 São Carlos - SP, Brazil.
[b]*Nanotechnology National Laboratory for Agriculture (LNNA), Embrapa Instrumentação, 13560-970 São Carlos -SP, Brazil*
[c]Institute of Chemistry, São Paulo State University, 14800-060 Araraquara-SP, Brazil.

KEYWORDS: self-assembled monolayers, immunosensor, ferrocene, and capacitance.

Highlights

- Peptides are suitable platform for use in electrochemical immunosensors.
- Immunosensor was intrinsically interrelated to peptide sequence.
- Capacity shown for a portable sensor for CRP and other biomarkers to pM level.
- Detection limit decreases with the heterogeneity index

ABSTRACT: Peptides with an active redox molecule are incorporated into nanostructured films for electrochemical biosensors with stable and controllable physicochemical properties. In this study, we synthesized three ferrocene (Fc)-containing peptides with the sequence Fc-Glu-$(Ala)_n$-Cys-NH_2, which could form self-assembled monolayers on gold and be attached to antibodies. The peptide with two alanines (n = 2) yielded the immunosensor with the highest performance in detecting C-reactive protein (CRP), a biomarker of inflammation. Using electrochemical impedance-derived capacitive spectroscopy, the limit of detection was 240 pM with a dynamic range that included clinically relevant CRP concentrations. With a combination of electrochemical methods and polarization-modulated infrared reflection-absorption spectroscopy, we identified the chemical groups involved in the antibody-CRP interaction, and were able to relate the highest performance for the peptide with n = 2 to chain length and efficient packing in the organized films. These strategies to design peptides and methods to fabricate the immunosensors are generic, and can be applied to other types of biosensors, including in low cost platforms for point-of-care diagnostics.

INTRODUCTION

Early detection of disease requires new devices that should be inexpensive, easy to handle outside of specialized laboratories (i.e. point-of-care), and have rapid, sensitive and selective responses [1–3]. These stringent requirements can be fulfilled with capacitive immunosensors made of nanostructured peptide films containing an active redox molecule whose physicochemical properties are stable and controllable. Nanostructured peptide films are suitable for immobilizing biomolecules capable of molecular recognition of a variety of biomarkers [4–7]. The advantages of peptides include design flexibility, easy synthesis, strong thiol-gold interactions (via cysteine residues) [4,8,9], and an ability to self-assemble into stable monolayers [10,11]. Indeed, peptide-based sensors have been used to detect cells, proteins, antibodies, ions and small molecules [10,12–15]. The principle of detection in peptide-containing sensors varies, including electrochemical methods as immunosensors for monitoring food safety, the environment, and in clinical diagnostics [16–19]. Electrochemical biosensors using peptides can detect various biomarkers [13,20–23], including metalloproteinases (biomarkers for cancer) [24], heavy metals [25], dengue biomarkers [26], and can also be used in e-noses [27]. As electrode modifiers, peptides do not only provide a large active surface area, but also facilitate electron transfer at the sensing interface, thereby imparting a high sensitivity. When

redox tags incorporated in the peptide backbone are employed as anchoring sites, the controlled immobilization and orientation of the probes may allow for efficient biorecognition, which further improves sensitivity.

An example of a peptide-based biosensor has been reported with the sequence Fc-Glu-Ala-Ala-Cys-NH_2 used in a matrix coupled with a DNA aptamer as a bioreceptor to detect the C-reactive protein (CRP), a biomarker of inflammation. This system had a limit of detection (LoD) of 7.2 pM and sensitivity of 87.7 % per decade. In this study, we extend this strategy with two other peptides in immunosensors for quantifying CRP; however, the peptides were designed to attach to antibodies rather than aptamers [28]. For the selection of peptides to be synthesized, we followed a set of design principles. First, an amide group was chosen for the C-terminus group to avoid repulsion between negative charges and side reactions during antibody coupling. A cysteine residue was used at the C-terminus with the sulfhydryl group serving to bind covalently to the gold electrode. Glutamic acid residues at the N-terminus were chosen to bind the electroactive compound ferrocene (Fc) in the amine group for attaching the antibody via the carboxyl group. This is convenient because the same peptide can be used for any bioreceptor [29]. In between the cysteine and glutamic acid residues, non-polar alanine residues were inserted to form a hydrophobic layer [30]. The amino acid alanine was selected due to its hydrophobicity and side chain volume [30,31]. Ferrocene was located at the N-terminal, thus decreasing steric hindrance between the peptides in their molecular organization over the gold electrode [11]. Using impedance-derived capacitive spectroscopy [32] as the principle of detection, we compared the performance of the film architectures of three peptides which differed from each other by the number of alanine groups (1 to 3). The method has the advantage of eliminating the need of a redox probe in the biological matrix or in the electrolyte, being which also makes it suitable for multiplexing in point-of-care applications. The film architectures were characterized by electrochemical and vibrational spectroscopy techniques in order to explain the different performances of the immunosensors and determine the main interactions responsible for immunosensing.

MATERIALS AND METHODS

2.1 Synthesis of redox-tagged peptides. All peptides were synthesized by solid phase peptide synthesis (SPPS) using Fmoc protocols in accordance with previous publications [11,28,33,34]. Table 1 and Figure S1 show the characteristics of the peptides.

2.2 Electrochemical measurements. The protocols for the measurements performed in this work are the same as reported by Piccoli and co-workers [11,28]. Gold electrodes were electrochemically polished in 0.5 M NaOH between –0.7 V and –1.7 V (500 cycles). An Autolab potentiostat (METROHM – Riverview, FL - USA) was employed for electrochemical measurements with a three-electrode cell consisting of a 2.0 mm diameter gold working electrode, a platinum mesh counter electrode, and an Ag|AgCl (3 M KCl) reference electrode. The measurements were performed in a cell containing 20 mM $TBAClO_4$ supporting electrolyte dissolved in acetonitrile and H_2O (20:80) volume (%) without any redox probe. The impedance spectra were recorded from 100 kHz to 0.1 Hz, from which the capacitance was calculated [35,36] using equation (1):

$$C^*(\omega) = 1/i\omega\, Z^*(\omega) \qquad (1)$$

where ω is the angular frequency and i is the complex number =√(-1) [37].

2.3 Fabrication of the immunosensors. CRP immunosensors were prepared by immersing clean Au electrodes in a solution containing 2 mM of each redox-tagged peptide in H_2O/ACN (50:50) for 16 h (25 °C). After rinsing thoroughly with deionized water, the δ-carboxyl group of glutamic acid was activated with a solution containing 0.4 M N-(3-dimethylaminopropyl)-N′-ethylcarbodiimide (EDC) and 0.1 M N-hydroxysuccinimide (NHS) for 30 min. EDC couples to the carboxyl groups of NHS, which forms an ester group that is more stable than the O-acylisourea intermediate, and allows for efficient conjugation to primary amines [29]. This step was followed by washing to remove unreacted EDC/NHS. Incubation with 1 µM of polyclonal anti-CRP IgG antibodies was performed in phosphate buffered saline (PBS) for 1 h. Cyclic voltammetry (CV) and electrochemical impedance spectroscopy (EIS) were conducted to confirm antibody immobilization. The final step involved incubation in 0.1% of bovine serum albumin (BSA) solution for 30 min to deactivate the active groups and prevent non-specific adsorption. Detection was performed with CRP in phosphate buffer solution (pH 7.4) at concentrations ranging from 0.5 nM to 10 nM. The incubation time was 30 min for each concentration and the electrodes were washed with PBS before electrochemical analysis. The calibration plot was calculated from the signal of relative response at any given CRP concentration as described by Piccoli et al [28]:

$$RR\%_{CRP} = ((RR_{CRP} - RR_{Blank}) / RR_{Blank}) \times 100 \quad (2).$$

where RR_{CRP} is the inverse of redox capacitance ($1/C_r$) at a specific concentration of CRP.

2.4 Mechanism of detection. The mechanism involved in the interaction between peptide films, antibodies, and antigens was analyzed using polarization-modulated infrared reflection-absorption spectroscopy (PM-IRRAS). A PMI 550 spectrophotometer (KSV Instruments, Helsinki, Finland), comprised of an infrared source, a ZnSe crystal photoelastic modulator, and a HgCdTe detector (model PCI-3TE-10.6), with an incident light angle of 81° and a spectral resolution of 8 cm^{-1} was used. These data were compared with the analytical parameters (LoD, silhouette coefficient, PM-IRRAS band area) of the immunosensors to understand the performance of the peptide films.

2.5 Data Analysis. Multiple sensing data normally possess high dimensionality, making it more difficult to extract useful information. For example, with EIS, data have more than 100 dimensions which are the number of frequencies (from 100 kHz to 0.1 Hz) used in real (Z') and imaginary (Z") impedance measurements. To reduce dimensionality while preserving similarity relationships and allow for a more detailed analysis of the sensitivity and selectivity, multidimensional projection techniques, such as interactive document mapping (IDMAP) [38], were applied. With IDMAP, a visualization map is obtained that permits analysis of global similarity relationships between different types of samples. We used IDMAP implemented in the Projection Explorer Sensors (PEx-Sensors) software, which considers the Euclidean distance between the electrochemical impedance spectra of different CRP protein concentrations X={x_1, x_2, …, x_n} in the original space to project the data instances onto a lower-dimension space, where Y={y_1, y_2, y_3, …, y_n) represents the mapping of X [38–40]. The function minimizes the term $\left|\delta\left(x_i, x_j\right) - d\left(y_i - y_j\right)\right| \forall x_i, x_j \in X$ and is given by following equation:

$$S_{IDMAP} = \frac{\delta(x_i, x_j) - \delta_{\min}}{\delta_{\max} - \delta_{\min}} - d(y_i, y_j) \quad (3)$$

where $\delta_{\max}$ and $\delta_{\min}$ are the maximum and minimum distances in the original spaces, $\delta(x_i, x_j)$ and $d(y_i, y_j)$ are the Euclidean distance between two samples in the original and projected spaces, respectively.

RESULTS AND DISCUSSION

3.1 Rationale in the choice of peptides. The primary aim in this work was to investigate whether biosensing performance could be optimized by altering amino acids in the peptide Fc-Glu-Ala-Ala-Cys-NH_2 (Peptide 2, Figure 1), which has already been used in the matrix of a biosensor [28]. Since the matrix comprises a self-assembled monolayer, an important requirement for the peptide is the ability to form intermolecular (interchain) hydrogen bonding. Peptide sequences with non-polar amino acids (valine, alanine and leucine) are known to self-assemble via hydrophobic effects [41]. The work by Nowinski and collaborators [30] with proline and glycine sequences showed that peptides containing hydrophobic residues could form self-assembled monolayers (SAMs) with well-ordered structures and high surface density. Therefore, we selected alanine to combine hydrophobicity and chain flexibility [30]. The peptides synthesized were labelled Peptide 1, 2 and 3 corresponding to the number of alanine residues (Figure 1). Peptide 2 is the same as in reference [28], but a new procedure was employed, and an antibody was used to detect CRP instead of an aptamer. Table 1 shows yields of 10, 12 and 16% for peptides containing three, two and one alanine residue, respectively, which are higher than that obtained for the earlier synthesis of Peptide 2 (5.3%) [28]. The position of ferrocene coupling was crucial for increasing the yield, as inferred from the lower yield due to steric hindrance with coupling in the middle of the main chain [11,42].

Figure 1 here

Table 1. Physicochemical properties, purity, and synthesis yield of the peptides.

Peptide	Molecular Weight (g moL^{-1})	Purity (%)	Retention Time (min)	Synthesis Yield (%)
1. Fc-Glu-Ala-Cys-NH_2	560.0	> 98	14.3	16
2. Fc-Glu-Ala-Ala-Cys-NH_2	632.6	> 98	15.5	12
3. Fc-Glu-Ala-Ala-Ala-Cys-NH_2	702.0	> 98	16.1	10

3.2 Electrochemical characterization of peptides.

Peptides immobilized onto gold electrodes exhibited reversible redox processes, as illustrated in Figure S2. This indicates that the reduced and oxidized forms of ferrocene were adsorbed in a well-packed SAM [35,42,43]. The peaks for Peptides 1 and 3 were less sharp than for Peptide 2, owing to kinetic and thermodynamic dispersions caused by self-interaction between the Fc groups, heterogeneous binding of the peptides on gold, or film defects [5,43,44]. Table 2 shows the formal potentials (Faradaic region) calculated as the average of the anodic and cathodic peak potentials E_{pa} and E_{pc}, and the peak separations ΔEp calculated as the difference E_{pa} – E_{pc} [5,45]. Peak separation increased at high scan rates, and were practically zero at small rates because the redox center was adsorbed on the electrode and diffusion did not play a role [46,47]. The Faradaic activity of redox-SAMs showed a formal potential (E_{in}) between 346 and 375 mV, with peak separation between 7 and 20 mV.

Table 2. Voltammetry characteristics of peptide films

Peptide	j_{cp} (μA·cm^{-2})	j_{ap} (μA·cm^{-2})	j_{ap}/j_{cp}	E_{cp} (mV)	E_{ap} (mV)	ΔE (mV)
1	–24.77	23.36	0.94	344	359	15
2	–41.26	41.38	1.00	358	378	20
3	–26.46	29.73	1.12	368	385	17

Surface molecular coverage was calculated from the cyclic voltammograms by determining the charge associated with ferrocene oxidation as follows:

$$Q = \frac{1}{\nu}\int iV'dV' \qquad (4)$$

This corresponds to the area of a CV peak divided by the scan rate v (100 mV·s^{-1}). Table 3 shows surface coverage for the SAM peptide films for the three peptides compared with the value for a mixed monolayer ((3 ± 1) × 10^{-10} mol·cm^{-2}) of acyl thiols [48,49]. The redox capacitance inferred from the CV data confirmed that alanine-containing peptides should be more efficient than isoleucine peptides due to the smaller surface coverage of 8 × 10^{-11} mol·cm^{-2} promoted by the side chain of isoleucine. This smaller coverage could be explained by steric hindrance between the peptides in their molecular organization. The redox capacitance for each monolayer was proportional to the molecular coating, i.e., the denser the packing, the higher the redox signal. The electron transfer constant is also an indicator of redox process efficiency (see section S2 for further details). This constant varied from 10.55 s^{-1} to 11.50 s^{-1} for the peptides, depending on the environment in which the redox probe was located. Chains with ferrocene further away from the gold electrode usually had lower electron transfer constants [43]. The dependence of the electron transfer rate on peptide length is exemplified by the value of K_{et}=

6870 s^{-1} for the 6-mer peptide containing (Ala-Aib) and K_{et}= 1.39 s^{-1} for the 24-mer [31]. PyMol software was used to calculate the ferrocene distance between the gold electrode and the antibody for the three film architectures. This approach used a reference amino acid with pairwise distances calculated between the atom taken as reference and all atoms within a given range. The distances between the electrode and the antibody (Fc distance) for the films were 1.21, 1.60, 1.83 nm for the architectures with Peptides 1, 2 and 3, respectively. The electron transfer rate shown in Table 3 was only slightly higher for the film with Peptide 2, which indicated that the addition or removal of an alanine residue had little effect. This is likely because the peptides have the same amino acid alanine as the organic structure (primary sequence), with no different amino acids included. These electron transfer rates were close to the value for the monolayer of a mixed 15-carbon chain acyl thiol, which was 12 s^{-1} [43,46]. The electrochemical properties of the films were similar, indicating that they did not depend only on the Fc distance to the electrode. Indeed, as seen in Table 3, the surface coverage varied significantly, with a much larger value for Peptide 2. This was related to film organization, which we confirmed with PM-IRRAS (see section 3.4).

Table 3. Electrochemical characteristics of the peptide films

Peptide	Half-Wave Potential (V)	Ferrocene Distance (nm)	Surface Coverage (mol·cm^{-2})	Redox Capacitance (μF·cm^{-2})	Electron Transfer Rate (s^{-1})
1	0.38	1.21	(1.80 ± 0.70) x 10^{-10}	(182.00 ± 4.98)	(11.00 ± 0.38)
2	0.36	1.60	(2.13 ± 0.70) x 10^{-10}	(300.00 ± 17.10)	(11.50 ± 0.71)
3	0.35	1.83	(1.20 ± 0.20) x 10^{-10}	(226.40 ± 1.40)	(10.55 ± 0.38)

3.3 Analytical performance of ferrocene peptide SAMs as capacitive platforms for CRP detection. CV and EIS were used to monitor the immunosensor fabrication process at each step. The results were corroborated by AFM images, as shown in Figure S3. Surface roughness increased due to two processes: immobilization of Peptide 2 on the gold surface and interaction of the anti-CRP antibody with the peptide film surface, which increased roughness by 90% and 260%, respectively. Orientation-controlled immobilization through carboxylic acids in the peptide chain with amine groups in the antibody Fc region permits enhanced antigen binding [50], which is reflected by electrode surface homogeneity after immobilization of the active layer. Figure 2a shows capacitance data for the immunosensor made with Peptide 2 (Fc-Glu-Ala-Ala-Cys-NH_2), which exhibited the highest performance. The capacitance changes shown in Figure 2a indicate that antibodies were successfully attached on the peptide SAMs via coupling using EDC/NHS, where the carboxylic acid groups of SAMs interact with the amine residues of antibodies [51]. Capacitance decreased due to antibody immobilization on the peptide films with the creation of a kinetic barrier between the redox probe in the peptide and the antibody [21,52]. Only small changes were observed after BSA incorporation to prevent non-specific adsorption. Detection of CRP is depicted in Figure 2b, with the capacitance decreasing with increasing CRP concentrations due to a lowered electron transfer rate. A linear relationship between 0.5 nM and 10 nM was obtained for the relative signal against the logarithm of CRP concentration and is shown in Figure S4. This linear dependence also applied to the immunosensors built with Peptide 3 but not with Peptide 1. The analytical characteristics are compiled in Table 4, with LoD calculated as the standard deviation (SD) of the blank response and the slope of the analytical curve ((3.3 SD)/B), where SD is the standard deviation of the blank measurements and B is the slope of the linear response [53]. The dynamic range confirmed the ability of

immunosensors containing Peptide 2 and 3 to detect CRP in a clinically-relevant range (0.5 – 1.0 mg·mL^{-1}) [54]. The immunosensors with Peptide 2 and Peptide 3 showed similar responses, but the sensitivity (3.7% per decade) for Peptide 3 (Fc-Glu-Ala-Ala-Ala-Cys-NH_2) was lower than the 11.4% per decade for Peptide 2 (Fc-Glu-Ala-Ala-Cys-NH_2). The lower sensitivity for Peptide 3 could be attributed to the increased distance for electron transfer with the ferrocene located at the N-terminal of the peptide, as film thickness increased with the additional alanine. In addition, Peptide 2 possessed a more structured film that facilitated antibody attachment to recognize CRP, as was demonstrated with PM-IRRAS in the next section.

Figure 2 here

Table 4: Analytical parameters for electrochemical detection of CRP using the antibody redox-peptide SAMs approach. Error bars represent one standard deviation of measurements on three separate electrodes.

Parameters	Peptide 1	Peptide 2	Peptide 3
Dynamic range (nmoL·L^{-1})	0.5-10	0.5-10	0.5-10
R^2	ND	0.99	0.97
Sensitivity per decade (%)	ND	11.4	3.7
LOD (nM)	ND	0.24	0.30
K_a	ND	$(5.9 \pm 0.3) \times 10^8$	$(1.7 \pm 0.3) \times 10^8$

As shown in Figure S4, the immunosensor containing Peptide 2 was selective toward CRP. Significant capacitance change was observed when CRP was present in the PBS solution, but the changes were negligible if BSA was used. We also confirmed with additional experiments that the film architecture fabricated with Peptide 1 (Fc-Glu-Ala-Cys-NH_2) could not be used to detect CRP. Figure S5 shows very small changes in capacitance when the antibody was immobilized on the peptide film. When the film was subjected to either PBS solutions or to different concentrations of CRP in PBS, the changes in capacitance were not higher in CRP (Figure 3). This is in contrast to the expectation for an immunosensor. Therefore, either the anti-CRP antibodies were not immobilized on the film or the peptide monolayer was not sufficiently organized to allow for antibody-CRP interaction. Together with the PM-IRRAS data presented below, we inferred that antibody immobilization took place, but the film was not as organized as for the other peptides.

Figure 3 here

The different performances of the three film architectures were assessed quantitatively by plotting the electrochemical impedance spectra using the multidimensional projection technique IDMAP [38], and determining the silhouette coefficient. The maps in Figure 4 represent the capacitance spectra for each film architecture subjected to different concentrations of CRP. A clear distinction between the data points was observed for the film with Peptide 2. In contrast, the distinction was less clear for the film with Peptide 3 and poor for the film with Peptide 1. The distinguishing ability can be quantified through the silhouette coefficient (*S*) defined in equation

(5) [55].

$$S = \frac{1}{n}\sum_{i=1}^{n}\frac{b_i - a_i}{\max(a_i, b_i)} \quad (5)$$

S ranges from –1 to 1, where values close to 1 are useful for discrimination, values close to –1 hinder distinction, and values close to 0 are indifferent for their distinguishing ability [38]. The film with Peptide 2 had an *S* of 0.904, with excellent distinction up to a concentration of 10 nM (red region). *S* was 0.309 and 0.214 for the film architectures containing Peptides 3 and 1, respectively.

Figure 4 here

The superior performance of the immunosensor made with Peptide 2 may be attributed to two factors: the first is the length of the peptide chain, which is approximately 16 Å, while Peptide 3 Fc-Glu-Ala-Ala-Ala-Cys-NH2) is 18 Å [9,56,57]. This difference in length allows the accumulated charge on the redox probe in the smaller chain to be more easily felt by the immunosensor, particularly in electron transfer to gold during antigen-antibody recognition. This is demonstrated by the larger variations of redox capacitance for Peptide 2, and is consistent with results for a mixed 11-carbon monolayer used in biosensors whose chain size is approximately 15 Å [11]. The second factor is the surface coverage (see Table 3) which is dependent on peptide organization and discussed in connection with the PM-IRRAS data. The limit of detection and sensitivity of the immunosensor containing Peptide 2 are competitive with other biosensors reported in the literature, as can be seen in Table S1.

The analytical plots taken from the capacitance data in Figure 2 at a fixed frequency of 0.1 Hz indicate that the relative change increased with CRP concentration (Figure 5). These curves can be fitted with the Langmuir-Freundlich model [1,58]. The Langmuir model is based on homogeneous binding sites, while the Freundlich model involves heterogeneous binding [59–61]. The Langmuir–Freundlich (LF) can provide heterogeneity information and is able to model adsorption behaviour over the entire concentration region up to saturation. The reason why a simple model like LF is suitable to fit the data arises from the predominance of specific interactions in the antibody−antigen pairs and/or peptide film/antibody dominating over all other possible interactions. The fitting parameters for Peptide 2 were Q_{sat} = 0.27 ± 0.06 pM, taken to be proportional to the amount of material adsorbed, and a heterogeneity index (n) of 0.84 ± 0.19. The linear regression constant was 0.99.

Figure 5 here

3.4 Mechanism behind CRP detection. With electrochemical measurements, we found that immunosensors can detect CRP at clinically-relevant levels, but no information was provided about the detection mechanism. CRP is a pentameric protein with identical non-covalently bound subunits of 206 amino acid residues and a molecular weight of ca. 23 kDa. Its detection using immunosensors should depend on specific association with antibodies via hydrogen bonds, hydrophobic interactions, electrostatic forces, and van der Waals forces. The PM-IRRAS technique was utilized to interrogate such interactions. Figure 6 shows a PM-IRRAS spectra

between 1500-1800 cm^{-1} containing amide I and amide II bands from the peptides, antibodies, and CRP. The amide I band appeared between 1600–1700 cm^{-1}, and was associated with 80% C=O stretching, 10% C−N stretching and 10% N−H bond vibration. The amide band II was observed at 1500–1600 cm^{-1} due to 60% N−H bond and 40% C−N bond stretching [62,63]. The immunosensor containing Peptide 2 (Fc-Glu-Ala-Ala-Cys-NH_2) and 3 (Fc-Glu-Ala-Ala-Ala-Cys-NH_2) showed an increase in band area and peak intensity of amide I and II, with antibody and antigen adsorption on the film surface (see Figure S6). The intensity of a band in a PM-IRRAS spectrum depends not only on the surface density of the group to which the band is assigned, but also on the orientation of the group dipole moment [39,64,65]. This latter dependence is the reason why bands can be upward or downward in a spectrum. Therefore, the monotonic increase in band area with CRP concentration in the immunosensors containing Peptide 2 and Peptide 3 indicates that the groups responsible for the amide I and amide II bands are not significantly reoriented, at least not to the extent that would prevent monotonic behaviour. Furthermore, there was no significant shift in the amide bands upon interaction with CRP. In contrast, for the film containing Peptide 1, the amide I band increased in intensity while the amide II band decreased upon interacting with CRP. In addition, there was a significant shift for these bands. One may thus infer that Peptide 1 did not form an organized film with possible CRP interpenetration, which would affect the orientation of amide II groups.

Figure 6 here

The average tilting angle of the peptide chain in relation to the substrate surface can be estimated from the ratio between the intensities of the amide I and amide II bands (see Supporting Information S4) [66]. The values obtained were 40.6°, 47.8°, and 43.5° for Peptides 1, 2, and 3, respectively. The peptides are therefore not parallel to the surface, and the larger average tilting angle for Peptide 2 is indicative of a more organized film. Indeed, the tilting angles increased according to the ability of the film architecture to detect CRP. Taken together, the PM-IRRAS results for the three film architectures indicate that immunosensing is only effective when the films are sufficiently organized to keep the peptide orientation during interaction with CRP. These results are consistent with the parameters derived from the other types of analysis (Table 5), including the silhouette coefficient, heterogeneity index inferred from the fitting of electrochemical data with the Langmuir-Freundlich model, and analytical performance of the immunosensors.

Table 5: Comparison of parameters inferred from PM-IRRAS results, electrochemical detection, and fitting with the Langmuir-Freundlich model for the three film architectures

Peptide Film Sequence	Silhouette Coefficient	Heterogeneity Index	Amide I PM IRRAS Band Area (AG-AB)	Amide II PM IRRAS Band Area (AG-AB)	LoD (pM)	Redox Capacitance ($\mu F \cdot cm^{-2}$)	Average Tilting Angle (°)
Fc-Glu-Ala-Cys-NH_2	0.214	---	0.67	-1.47	---	182.0 ± 4.9	40.6
Fc-Glu-Ala-Ala-Cys-NH_2	0.904	0.842	0.79	0.42	240	226.4 ± 1.4	47.8
Fc-Glu-Ala-Ala-Ala-Cys-NH_2	0.390	0.141	0.71	0.66	300	243.9 ± 1.9	43.5

CONCLUSIONS

We explored the possible control of molecular architecture in nanostructured peptide films in immunosensors to detect CRP. Two of the peptides synthesized, Peptide 2 and Peptide 3, were suitable to build electrochemical immunosensors, while Peptide 1 was not. Two factors were found to determine this suitability: the distance between the Fc region and the electrode, and the peptide organization in the film. Peptide 1, for example, had the shortest chain but did not form an organized film according to the PM-IRRAS results. This also affected surface coverage and consequently the electrochemical signal. The highest performance was obtained with Peptide 2, whose chain length seems appropriate for an efficient electron transfer as reported in another work with biosensors [28], and had the largest average tilting angle in the organized film. Significantly, the immunosensor with Peptide 2 had sufficient sensitivity to detect CRP in clinically-relevant concentrations and was proven to exhibit selectivity. The sensing performance with fast response makes this immunosensing technology based on peptide nanostructured films promising for point-of-care devices [67], as the sensing units may be integrated into lab-on-chip (LOC) platforms. It is also worth mentioning that the combination of characterization techniques and tools for data analysis employed in this work may be replicated in other biosensing devices with possible tuning of electrochemical properties.

ASSOCIATED CONTENT

Supporting Information

Further information about characterization of peptide films and immunosensors performance can be found in the SI.

AUTHOR INFORMATION

Corresponding Author

*eduardo.cilli@unesp.br; tel: +55-16-33019679, Instituto de Química, Universidade Estadual Paulista, 14800-900 Araraquara-SP, Brazil.

*chu@ifsc.usp.br; tel: +55-16-3373-9672, IFSC - Instituto de Física de São Carlos – USP, 13566-590, São Carlos - SP,Brazil.

Notes

The authors declare no competing financial interest.

Present Address

†Julia P Piccoli is currently at Instituto Vita Nova. Rua Barão de Itapura, 135, CEP: 13186-432, Parque Odimar, Hortolândia, São Paulo, Brazil.

ACKNOWLEDGMENT

CNPq, CAPES and FAPESP (2018/22214-6, 2017/24839-0, 2013/07600-3, 2018/18953-8 and 2018/18231-2) supported the work. EMC is a senior researcher of the CNPq (grant 301975/2018-3).

The authors acknowledge Prof. Paulo Bueno for support at the electrochemical laboratory.

REFERENCES

[1] J.C. Soares, A.C. Soares, P.A.R. Pereira, V. da C. Rodrigues, F.M. Shimizu, M.E. Melendez, C. Scapulatempo Neto, A.L. Carvalho, F.L. Leite, S.A.S. Machado, O.N. Oliveira, Adsorption according to the Langmuir–Freundlich model is the detection mechanism of the antigen p53 for early diagnosis of cancer, Phys. Chem. Chem. Phys. 18 (2016) 8412–8418. doi:10.1039/C5CP07121F.

[2] J.C. Soares, L.E.O. Iwaki, A.C. Soares, V.C. Rodrigues, M.E. Melendez, J.H.T.G. Fregnani, R.M. Reis, A.L. Carvalho, D.S. Corrêa, O.N. Oliveira, Immunosensor for Pancreatic Cancer Based on Electrospun Nanofibers Coated with Carbon Nanotubes or Gold Nanoparticles, ACS Omega. 2 (2017) 6975–6983. doi:10.1021/acsomega.7b01029.
[3] J. Wang, Nanomaterial-based electrochemical biosensors, Analyst. 130 (2005) 421–426. doi:10.1039/B414248A.
[4] Y. Wu, F. Wang, K. Lu, M. Lv, Y. Zhao, Self-assembled dipeptide-graphene nanostructures onto an electrode surface for highly sensitive amperometric hydrogen peroxide biosensors, Sensors Actuators, B Chem. 244 (2017) 1022–1030. doi:10.1016/j.snb.2017.01.048.
[5] E. Gatto, M. Caruso, M. Venanzi, Handbook of Nanoelectrochemistry, 2016. doi:10.1007/978-3-319-15207-3.
[6] H. Etayash, Real-time Detection of Breast Cancer Cells Using Peptide functionalized Microcantilever Arrays, Scientific Reports, 2015.
[7] H.S. Mandal, H.B. Kraatz, Electron transfer across α-helical peptides: Potential influence of molecular dynamics, Chem. Phys. 326 (2006) 246–251. doi:10.1016/j.chemphys.2006.01.010.
[8] Q. Yang, L. Wang, W. Lin, G. Ma, J. Yuan, S. Chen, W.L. Yang Qinghua, Development of nonfouling polypeptides with uniform alternating charges by polycondensation of the covalently bonded dimer of glutamic acid and lysine, J. Mater. Chem. B. 2 (2014) 577–584. doi:10.1039/c3tb21333a.
[9] O.R. Bolduc, C.M. Clouthier, J.N. Pelletier, J.F. Masson, Peptide self-assembled monolayers for label-free and unamplified surface plasmon resonance biosensing in crude cell lysate, Anal Chem. 81 (2009) 6779–6788. http://www.ncbi.nlm.nih.gov/pubmed/19606821.
[10] A. Shah, B. Adhikari, S. Martic, A. Munir, S. Shahzad, K. Ahmad, H.B. Kraatz, Electron transfer in peptides, Chem Soc Rev. 44 (2015) 1015–1027. https://www.ncbi.nlm.nih.gov/pubmed/25619931.
[11] J.P.P. Piccoli, A. Santos, N.A.A. Santos-Filho, E.N.N. Lorenzón, E.M.M. Cilli, P.R.R. Bueno, The self-assembly of redox active peptides: Synthesis and electrochemical capacitive behavior, Biopolymers. (2016). doi:10.1002/bip.22815.
[12] N. Liu, J. Song, Y. Lu, J.J. Davis, F. Gao, X. Luo, Electrochemical Aptasensor for Ultralow Fouling Cancer Cell Quantification in Complex Biological Media Based on Designed Branched Peptides, Anal. Chem. (2019) acs.analchem.9b01129. doi:10.1021/acs.analchem.9b01129.
[13] Y.M. Lei, M.M. Xiao, Y.T. Li, L. Xu, H. Zhang, Z.Y. Zhang, G.J. Zhang, Detection of heart failure-related biomarker in whole blood with graphene field effect transistor biosensor, Biosens. Bioelectron. 91 (2017) 1–7. doi:10.1016/j.bios.2016.12.018.
[14] S. Pavan, F. Berti, Short peptides as biosensor transducers., Anal. Bioanal. Chem. 402 (2012) 3055–70. doi:10.1007/s00216-011-5589-8.
[15] A. Parnsubsakul, R.E. Safitri, P. Rijiravanich, W. Surareungchai, Electrochemical assay of proteolytically active prostate specific antigen based on anodic stripping voltammetry of silver enhanced gold nanoparticle labels, J. Electroanal. Chem. 785 (2017) 125–130. doi:10.1016/j.jelechem.2016.12.010.
[16] D. Kang, S. Sun, M. Kurnik, D. Morales, F.W. Dahlquist, K.W. Plaxco, New Architecture for Reagentless, Protein-Based Electrochemical Biosensors, J. Am. Chem. Soc. 139 (2017) 12113–12116. doi:10.1021/jacs.7b05953.

[17] D. Deng, Y. Shi, H. Feng, Q. Chen, D. Li, L. Liu, Label-free electrochemical sensing platform for the detection of protease, Int. J. Electrochem. Sci. 8 (2013) 6933–6940.
[18] A. Florea, G. Melinte, I. Simon, C. Cristea, Electrochemical Biosensors as Potential Diagnostic Devices for Autoimmune Diseases, Biosensors. 9 (2019) 38. doi:10.3390/bios9010038.
[19] L. Fetter, J. Richards, J. Daniel, L. Roon, T.J. Rowland, A.J. Bonham, Electrochemical aptamer scaffold biosensors for detection of botulism and ricin toxins, Chem Commun. 51 (2015) 15137–15140. https://www.ncbi.nlm.nih.gov/pubmed/26323568.
[20] J. Scotchler, R. Lozier, A.B. Robinson, Cleavage of single amino acid residues from Merrifield resin with hydrogen chloride and hydrogen fluoride, J Org Chem. 35 (1970) 3151–3152. http://www.ncbi.nlm.nih.gov/pubmed/5450527.
[21] S. Martić, M. Labib, P.O. Shipman, H.-B.B. Kraatz, Ferrocene-peptido conjugates: from synthesis to sensory applications., Dalton Trans. 40 (2011) 7264–90. doi:10.1039/c0dt01707h.
[22] H. Etayash, K. Jiang, S. Azmi, T. Thundat, K. Kaur, Real-time detection of breast cancer cells using peptide-functionalized microcantilever arrays, Sci. Rep. 5 (2015) 1–13. doi:10.1038/srep13967.
[23] F. Meng, W. Liang, H. Sun, L. Wu, X. Gong, P. Miao, A Peptide-Based Electrochemical Biosensor for Facile Measurement of Whole-Blood Heparin, ChemElectroChem. 4 (2017) 472–475. doi:10.1002/celc.201600680.
[24] H. Xu, H. Ye, L. Yu, Y. Chi, X. Liu, G. Chen, Tailor-made peptide sensor for detection of matrix metalloproteinase 2 in blood serum, Anal. Methods. 7 (2015) 5371–5374. doi:10.1039/C5AY00666J.
[25] M. Siepi, R. Oliva, L. Petraccone, P. Del Vecchio, E. Ricca, R. Isticato, M. Lanzilli, O. Maglio, A. Lombardi, L. Leone, E. Notomista, G. Donadio, Fluorescent peptide dH3w: A sensor for environmental monitoring of mercury (II), PLoS One. 13 (2018) e0204164. doi:10.1371/journal.pone.0204164.
[26] J. Cecchetto, A. Santos, A. Mondini, E.M. Cilli, P.R. Bueno, Serological point-of-care and label-free capacitive diagnosis of dengue virus infection, Biosens. Bioelectron. 151 (2020) 111972. doi:https://doi.org/10.1016/j.bios.2019.111972.
[27] W. Wojnowski, T. Majchrzak, T. Dymerski, J. Gębicki, J. Namieśnik, Portable Electronic Nose Based on Electrochemical Sensors for Food Quality Assessment, Sensors (Basel). 17 (2017) 2715. doi:10.3390/s17122715.
[28] J. Piccoli, R. Hein, A.H.H. El-Sagheer, T. Brown, E.M.M. Cilli, P.R.R. Bueno, J.J.J. Davis, Redox Capacitive Assaying of C-Reactive Protein at a Peptide Supported Aptamer Interface, Anal. Chem. 90 (2018) 3005–3008. doi:10.1021/acs.analchem.7b05374.
[29] M.J. Fischer, Amine coupling through EDC/NHS: a practical approach, Methods Mol Biol. 627 (2010) 55–73. https://www.ncbi.nlm.nih.gov/pubmed/20217613.
[30] A.K. Nowinski, F. Sun, A.D. White, a J. Keefe, S. Jiang, Sequence, structure, and function of peptide self-assembled monolayers, J Am Chem Soc. 134 (2012) 6000–6005. doi:10.1021/ja3006868.
[31] D. Matsushita, H. Uji, S. Kimura, Effect of oscillation dynamics on long-range electron transfer in a helical peptide monolayer, Phys. Chem. Chem. Phys. 20 (2018) 15216–15222. doi:10.1039/C8CP02315H.
[32] A. Santos, J.J. Davis, P.R. Bueno, Fundamentals and Applications of Impedimetric and Redox Capacitive Biosensors, J Anal Bioanal Tech S. 7 (2014) 2.
[33] W.C. CHAN, P.D. WHITE, Fmoc Solid Phase Peptide Synthesis: A Practical Approach,

Oxford Univ. Press. (2000) 1–341.
[34] R.B. Merrifield, Solid Phase Peptide Synthesis. I. The Synthesis of, J. Am. Chem. Soc. 85 (1963) 2149. doi:10.1021/ja00897a025.
[35] J. Muñoz, R. Montes, M. Baeza, Trends in electrochemical impedance spectroscopy involving nanocomposite transducers: Characterization, architecture surface and bio-sensing, TrAC - Trends Anal. Chem. 97 (2017) 201–215. doi:10.1016/j.trac.2017.08.012.
[36] P.R. Bueno, J.J. Davis, Measuring quantum capacitance in energetically addressable molecular layers, Anal Chem. 86 (2014) 1337–1341. http://www.ncbi.nlm.nih.gov/pubmed/24405523.
[37] P.R. Bueno, G. Mizzon, J.J. Davis, Capacitance Spectroscopy : A Versatile Approach To Resolving the Redox Density of States and Kinetics in Redox-Active Self-Assembled Monolayers, J Phys Chem B. 116 (2012) 8822–8829. http://www.ncbi.nlm.nih.gov/pubmed/22686462.
[38] F. V. Paulovich, M.L. Moraes, R.M. Maki, M. Ferreira, O.N. Oliveira, M.C.F. De Oliveira, Information visualization techniques for sensing and biosensing, Analyst. 136 (2011) 1344–1350. doi:10.1039/c0an00822b.
[39] A.C. Soares, J.C. Soares, F.M. Shimizu, M.E. Melendez, A.L. Carvalho, O.N. Oliveira, Controlled Film Architectures to Detect a Biomarker for Pancreatic Cancer Using Impedance Spectroscopy, ACS Appl. Mater. Interfaces. 7 (2015) 25930–25937. doi:10.1021/acsami.5b08666.
[40] A.C. Soares, J.C. Soares, F.M. Shimizu, V. da C. Rodrigues, I.T. Awan, M.E. Melendez, M.H. de O. Piazzetta, A.L. Gobbi, R.M. Reis, J.H.T.G.J.H.T.G. Fregnani, A.L.A.L. Carvalho, O.N. Oliveira Jr., O.N. Oliveira, A simple architecture with self-assembled monolayers to build immunosensors for detecting the pancreatic cancer biomarker CA19-9, Analyst. 143 (2018). doi:10.1039/C8AN00430G.
[41] Y. Zheng, Y. Wen, A.M. George, A.M. Steinbach, B.E. Phillips, N. Giannoukakis, E.S. Gawalt, W.S. Meng, A peptide-based material platform for displaying antibodies to engage T cells, Biomaterials. 32 (2011) 249–257. doi:10.1016/j.biomaterials.2010.08.083.
[42] A. Santos, J.P.J.P.P. Piccoli, N.A.N.A. Santos-Filho, E.M.E.M. Cilli, P.R.P.R. Bueno, Redox-tagged peptide for capacitive diagnostic assays, 281–287. doi:10.1016/j.bios.2014.12.059.
[43] A.L. Eckermann, D.J. Feld, J.A. Shaw, T.J. Meade, Electrochemistry of redox-active self-assembled monolayers, Coord Chem Rev. 254 (2010) 1769–1802. http://www.ncbi.nlm.nih.gov/pubmed/20563297.
[44] S. Beheshti, S. Martić, H.-B. Kraatz, Hierarchical organization of ferrocene-peptides., Chemistry. 18 (2012) 9099–105. doi:10.1002/chem.201200666.
[45] E. Gatto, M. Venanzi, Self-assembled monolayers formed by helical peptide building blocks: A new tool for bioinspired nanotechnology, Polym. J. 45 (2013) 468–480. doi:10.1038/pj.2013.27.
[46] A.L. Eckermann, K.D. Barker, M.R. Hartings, M.A. Ratner, T.J. Meade, Synthesis and electrochemical characterization of a transition-metal-modified ligand-receptor pair, J Am Chem Soc. 127 (2005) 11880–11881. https://www.ncbi.nlm.nih.gov/pubmed/16117493.
[47] A.L. Eckermann, D.J. Feld, J.A. Shaw, T.J. Meade, Electrochemistry of redox-active self-assembled monolayers, Coord. Chem. Rev. 254 (2010) 1769–1802. doi:10.1016/j.ccr.2009.12.023.
[48] L. Newton, T. Slater, N. Clark, A. Vijayaraghavan, Self assembled monolayers (SAMs) on metallic surfaces (gold and graphene) for electronic applications, J. Mater. Chem. C. 1

(2013) 376–393. doi:10.1039/c2tc00146b.
[49] S. Dong, J. Li, Self-assembled monolayers of thiols on gold electrodes for bioelectrochemistry and biosensors, Bioelectrochemistry Bioenerg. 42 (1997) 7–13.
[50] A. Makaraviciute, A. Ramanaviciene, Site-directed antibody immobilization techniques for immunosensors, Biosens Bioelectron. 50 (2013) 460–471. https://www.ncbi.nlm.nih.gov/pubmed/23911661.
[51] S. Asiaei, B. Smith, P. Nieva, Enhancing conjugation rate of antibodies to carboxylates: Numerical modeling of conjugation kinetics in microfluidic channels and characterization of chemical over-exposure in conventional protocols by quartz crystal microbalance, Biomicrofluidics. 9 (2015) 64115. doi:10.1063/1.4937929.
[52] M. Cui, Y. Wang, M. Jiao, S. Jayachandran, Y. Wu, X. Fan, X. Luo, Mixed Self-Assembled Aptamer and Newly Designed Zwitterionic Peptide as Antifouling Biosensing Interface for Electrochemical Detection of alpha-Fetoprotein, ACS Sensors. 2 (2017) 490–494. doi:10.1021/acssensors.7b00103.
[53] G.L. Long, J.D. Winefordner, Limit of detection. A closer look at the IUPAC definition, Anal. Chem. 55 (1983) 712A–724A %@ 0003–2700.
[54] W. Ansar, S. Ghosh, C-reactive protein and the biology of disease, Immunol Res. 56 (2013) 131–142. https://www.ncbi.nlm.nih.gov/pubmed/23371836.
[55] A. Inselberg, B. Dimsdale, Parallel coordinates: a tool for visualizing multi-dimensional geometry, in: Proc. First IEEE Conf. Vis. Vis. `90, 1990: pp. 361–378. doi:10.1109/VISUAL.1990.146402.
[56] M. Venanzi, E. Gatto, F. Formaggio, C. Toniolo, The importance of being Aib. Aggregation and self-assembly studies on conformationally constrained oligopeptides, J. Pept. Sci. 23 (2017) 104–116. doi:10.1002/psc.2956.
[57] Effect of spacer length on the performance of peptide-based electrochemical biosensors for protease detection, Sensors Actuators B Chem. 255 (2018) 3040 – 3046. http://www.sciencedirect.com/science/article/pii/S0925400517317951.
[58] G.P. Jeppu, T.P. Clement, A modified Langmuir-Freundlich isotherm model for simulating pH-dependent adsorption effects, Sorption Transp. Process. Affect. Fate Environ. Pollut. Subsurf. 129–130 (2012) 46–53. doi:10.1016/j.jconhyd.2011.12.001.
[59] G. Ertürk, L. Uzun, M.A. Tümer, R. Say, A. Denizli, Fab fragments imprinted SPR biosensor for real-time human immunoglobulin G detection, Biosens. Bioelectron. 28 (2011) 97–104. doi:10.1016/j.bios.2011.07.004.
[60] V.K. Gupta, M.L. Yola, N. Atar, A novel molecular imprinted nanosensor based quartz crystal microbalance for determination of kaempferol, Sensors Actuators, B Chem. 194 (2014) 79–85. doi:10.1016/j.snb.2013.12.077.
[61] R.S. and D.P. and W.G.M. Kane, Kosmotropes Form the Basis of Protein-Resistant Surfaces, Langmuir. 19 (2003) 2388–2391.
[62] N.B. Colthup, L.H. Daly, S.E. Wiberley, CHAPTER 2 - IR EXPERIMENTAL CONSIDERATIONS, in: N.B. Colthup, L.H. Daly, S.E.B.T.-I. to I. and R.S. (Third E. Wiberley (Eds.), Academic Press, San Diego, 1990: pp. 75–107. doi:https://doi.org/10.1016/B978-0-08-091740-5.50005-3.
[63] N.B. Colthup, L.H. Daly, S.E. Wiberley, CHAPTER 4 - THE VIBRATIONAL ORIGIN OF GROUP FREQUENCIES, in: N.B. Colthup, L.H. Daly, S.E.B.T.-I. to I. and R.S. (Third E. Wiberley (Eds.), Academic Press, San Diego, 1990: pp. 171–213. doi:https://doi.org/10.1016/B978-0-08-091740-5.50007-7.
[64] M.J. Desroches, N. Chaudhary, S. Omanovic, PM-IRRAS investigation of the interaction

of serum albumin and fibrinogen with a biomedical-grade stainless steel 316LVM surface, Biomacromolecules. 8 (2007) 2836–2844. doi:10.1021/bm070289d.

[65] M.A. and L.B.G. and D.N. and B.B. and V.L. and B.T. Ramin, PM-IRRAS Investigation of Self-Assembled Monolayers Grafted onto SiO2/Au Substrates, Langmuir. 27 (2011) 6076–6084.

[66] E. Gatto, S. Kubitzky, M. Schriever, S. Cesaroni, C. Mazzuca, G. Marafon, M. Venanzi, M. De Zotti, Building Supramolecular DNA-Inspired Nanowires on Gold Surfaces: From 2D to 3D, Angew. Chemie - Int. Ed. 58 (2019) 7308–7312. doi:10.1002/anie.201901683.

[67] J.M. Lim, M.Y. Ryu, J.W. Yun, T.J. Park, J.P. Park, Electrochemical peptide sensor for diagnosing adenoma-carcinoma transition in colon cancer, Biosens. Bioelectron. 98 (2017) 330–337. doi:10.1016/j.bios.2017.07.013.

Insert Table of Contents artwork here